

Uncertainty Analysis of the Navier-Stokes Solver SURF for Two-Dimensional Steady Incompressible Flows

Kenichi Morimoto and Takanori Hino

National Maritime Research Institute, Center for CFD Research,
6-38-1 Shinkawa, Mitaka, Tokyo 181-0004, JAPAN
E-mail: morimoto@nmri.go.jp, hino@nmri.go.jp

I INTRODUCTION

In recent years, Computational Fluid Dynamics (CFD) has become a powerful tool for flow field analysis and is extensively applied to practical engineering problems such as the design of a ship hull form or other devices with complicated geometry. In order to promote its further development with well-established reliability, it is widely accepted that considerable efforts should be made for evaluating the accuracy of the CFD analysis. In general, CFD results of a specific problem depend much on the quality and size of the grid used. Therefore, the convergence behavior with qualified grids should be examined through successive grid refinement. Furthermore, the necessity of the numerical uncertainty estimation for the problem with exact solutions available has been strongly claimed as in the last workshop.

This paper reports the numerical uncertainty estimation of the two test case problems for the two-dimensional, steady, incompressible, turbulent flows: 1) the manufactured solution in a square domain recently proposed by Eça et al. [1], and 2) the turbulent flow over a backward facing step (ERCOFTAC Database, Case-30). The flow solver employed is the Navier-Stokes solver SURF, which is being developed toward a practical ship design tool at the National Maritime Research Institute (NMRI). The uncertainty estimation procedure proposed by Eça and Hoekstra [2, 3], which is based on the concept of Grid Convergence Index (GCI) proposed by Roache [4], is employed for the present analysis on both problems. The specific objectives of the present study are to investigate the grid convergence behavior and to verify and characterize the SURF solver.

The paper is organized as follows. In Sec. II, the numerical method of the present solver is outlined. The computational conditions including the boundary conditions and the uncertainty estimation procedure presently employed are described in Sec. III, followed by the results of the present analysis in Sec. IV. This paper is concluded in Sec. V.

II NUMERICAL METHOD

The SURF (Solution algorithm for Unstructured RaNS with FVM) solver is employed in this study. The governing equations are the three-dimensional Reynolds-averaged Navier-Stokes equations for incompressible flows. The coupling of the velocity and pressure fields is implemented with the artificial-compressibility concept proposed by Chorin [6]. The equations nondimensionalized by the reference density ρ_0 , velocity U_0 and length L_0 can be expressed in a vector form as follows:

$$\frac{\partial \mathbf{q}}{\partial t} + \frac{\partial(\mathbf{e} - \mathbf{e}^v)}{\partial x} + \frac{\partial(\mathbf{f} - \mathbf{f}^v)}{\partial y} + \frac{\partial(\mathbf{g} - \mathbf{g}^v)}{\partial z} = 0, \quad (1)$$

where the flow variables are denoted by

$$\mathbf{q} = [p \quad u \quad v \quad w]^T \quad (2)$$

with the pressure p and the velocity components u , v and w in the x -, y - and z - directions, respectively.

The inviscid fluxes \mathbf{e} , \mathbf{f} and \mathbf{g} are defined as:

$$\mathbf{e} = \begin{bmatrix} \beta u \\ u^2 + p \\ uv \\ uw \end{bmatrix}, \quad \mathbf{f} = \begin{bmatrix} \beta v \\ vu \\ v^2 + p \\ vw \end{bmatrix}, \quad \mathbf{g} = \begin{bmatrix} \beta w \\ wu \\ wv \\ w^2 + p \end{bmatrix} \quad (3)$$

with β being a parameter for artificial compressibility. The viscous fluxes \mathbf{e}^v , \mathbf{f}^v and \mathbf{g}^v are given by

$$\mathbf{e}^v = \begin{bmatrix} 0 \\ \tau_{xx} \\ \tau_{xy} \\ \tau_{zx} \end{bmatrix}, \quad \mathbf{f}^v = \begin{bmatrix} 0 \\ \tau_{xy} \\ \tau_{yy} \\ \tau_{yz} \end{bmatrix}, \quad \mathbf{g}^v = \begin{bmatrix} 0 \\ \tau_{zx} \\ \tau_{yz} \\ \tau_{zz} \end{bmatrix}, \quad (4)$$

where

$$\tau_{ij} = \left(\frac{1}{Re} + \nu_t \right) \left(\frac{\partial u_i}{\partial x_j} + \frac{\partial u_j}{\partial x_i} \right). \quad (5)$$

The Reynolds number Re is defined as $U_0 L_0 / \nu$ with the kinematic viscosity ν . The nondimensional kinematic eddy viscosity ν_t is determined by a turbulence closure model. In the present study, the original Spalart-Allmaras (SA) one-equation model [7] is employed. The transport equation for the working variable $\tilde{\nu}$ is written as follows:

$$\begin{aligned} \frac{\partial \tilde{\nu}}{\partial t} + u \frac{\partial \tilde{\nu}}{\partial x} + v \frac{\partial \tilde{\nu}}{\partial y} + w \frac{\partial \tilde{\nu}}{\partial z} = c_{b1} \tilde{S} \tilde{\nu} \\ + \frac{1}{\sigma} \left[\nabla \cdot \left(\left(\frac{1}{Re} + \tilde{\nu} \right) \nabla \tilde{\nu} \right) + c_{b2} (\nabla \tilde{\nu})^2 \right] \\ - c_{w1} f_w \left(\frac{\tilde{\nu}}{d} \right)^2 \end{aligned} \quad (6)$$

where $\tilde{\nu}$ is related to the eddy viscosity ν_t as

$$\nu_t = \tilde{\nu} f_{v1}, \quad f_{v1} = \frac{\chi^3}{\chi^3 + c_{v1}^3}, \quad \chi \equiv \frac{\tilde{\nu}}{\nu} \quad (7)$$

and

$$\tilde{S} = |\boldsymbol{\omega}| + \frac{\tilde{\nu}}{\kappa^2 d^2} f_{v2}, \quad f_{v2} = 1 - \frac{\chi}{1 + \chi f_{v1}}, \quad f_w = g \left[\frac{1 + c_{w3}^6}{g^6 + c_{w3}^6} \right]^{1/6} \quad (8)$$

with

$$g = r + c_{w2} (r^6 - r), \quad r \equiv \frac{\tilde{\nu}}{\tilde{S} \kappa^2 d^2} \quad (9)$$

In Eqs. (6-9), d and $|\boldsymbol{\omega}|$ denote the distance to the closest wall and the magnitude of the vorticity. The right-hand side terms of Eq. (6) represent the turbulent eddy viscosity production, diffusion, and near-wall destruction terms, respectively. The model constants are set equal to those of the original paper [7].

Spatial discretization is based on a cell-centered finite-volume method. A computational domain is divided into unstructured polyhedral cells, in which all the flow variables are stored. In the SURF solver, the cell shape can be arbitrary, i.e., hexahedra, tetrahedra, prisms or pyramids, but only the hexahedral cells are used for generating orthogonal grids in the present study.

The inviscid fluxes are evaluated by an upwind scheme based on the flux-difference splitting of Roe [8], and the second-order accuracy is achieved in the momentum equation by the MUSCL scheme [9]. The viscous fluxes are discretized by the second-order centered differencing method. For the time integration, the backward Euler scheme is employed. More details of the above procedure are available in Ref. [5].

III COMPUTATIONAL CONDITIONS

Problem Setting and Boundary Conditions

In order to simulate the turbulent flows for each test case problem, the following conditions are assumed in the present study.

A. Manufactured solution

The computational domain is defined by $0.5 \leq x \leq 1$ and $0 \leq y \leq 0.5$. The Reynolds number is set to 10^6 , and thus the nondimensional kinematic viscosity is 10^{-6} . The boundary conditions presently employed are summarized in Table 1. The subscript ms denotes the quantity of manufactured solutions. The Dirichlet boundary conditions are employed for the velocity and eddy-viscosity field at the wall ($y = 0$) and the inlet ($x = 0.5$). The Neumann boundary conditions are employed using exact solutions. For solving manufactured solutions, the source terms provided are added to the momentum equation (Eq. (1)) and the transport equation of $\tilde{\nu}$ (Eq. (6)). The following cases are considered independently in the present analysis.

Table 1. Boundary conditions for the manufactured solution.

	p	$\phi (= u, v, \nu_t)$
Wall ($y = 0$)	$\partial p / \partial n = 0$	$\phi = 0$
Inlet ($x = 0.5$)	$\partial p / \partial n = \partial p / \partial n _{ms}$	$\phi = \phi_{ms}$
Outlet ($x = 1$)	$\partial p / \partial n = \partial p / \partial n _{ms}$	$\partial \phi / \partial n = \partial \phi / \partial n _{ms}$
Top ($y = 0.5$)	$p = 0$	$\partial \phi / \partial n = \partial \phi / \partial n _{ms}$

A-1. Simulation of the velocity and pressure fields with fixed eddy-viscosity (MS1 & MS2)

For these conditions, only the momentum equations coupled with the continuity equation are solved to determine the velocity and pressure fields. The turbulent eddy-viscosity is prescribed using the manufactured solutions for the SA model. In Cases V(MS1) and V(MS2), the eddy-viscosity profile is given by MS1 and MS2, which are 1st (MS1) and 2nd (MS2) order manufactured solutions, respectively.

A-2. Simulation of the full flow field (MS1)

The complete flow field is computed with SA, by using the MS1 profile of the eddy-viscosity as the boundary condition. This case is referred to as VT(MS1) for the results shown later.

B. Backward facing step

The Reynolds number based on the reference velocity and the reference length (the step height) is set to 5×10^4 . At the inlet boundary, the Dirichlet conditions are imposed on the velocity and eddy-viscosity field, which are set to the prescribed inlet profiles provided. The Neumann boundary condition is employed for the pressure. At the outlet boundary, the Neumann condition is imposed on u , v and v_t , while p is set to zero. The non-slip condition is imposed on the walls.

Table 2. Boundary conditions for the backward facing step.

	p	$\phi (= u, v, v_t)$
Wall	$\partial p / \partial n = 0$	$\phi = 0$
Inlet ($x = -4h$)	$\partial p / \partial n = 0$	$\phi = \phi_{in}$
Outlet ($x = 40h$)	$p = 0$	$\partial \phi / \partial n = 0$

Uncertainty Estimation Procedure

The uncertainty estimation procedure proposed by Eça and Hoekstra [2, 3] is applied to all the test cases presented here. The estimation of the uncertainty U of the solution on a given grid is based on the Grid Convergence Index (GCI) method, i.e.,

$$U = F_s |\delta_{RE}|, \quad (10)$$

where F_s and δ_{RE} respectively denote a safety factor and the discretization error. The Richardson extrapolation is used to obtain the error as

$$\delta_{RE} = \phi_i - \phi_o = \alpha h_i^p, \quad (11)$$

where ϕ_i , ϕ_o , h_i , α and p represent the numerical solution on a given grid denoted by subscript i , the estimated exact solution, the representative grid cell size, a constant for the extrapolation, and the observed order of accuracy, respectively. The three unknowns, i.e., ϕ_o , α and p , are obtained by a least squares root approach. For $p \leq 0.5$ or $p > 2$, the error estimation is replaced by the following definition with fixed exponents:

$$\delta_{RE2} = \phi_i - \phi_o = \alpha_2 h_i^2 + \alpha_3 h_i^3. \quad (12)$$

In order to neglect the iterative uncertainty, all calculations were continued until the residual of all variables reduce to machine zero.

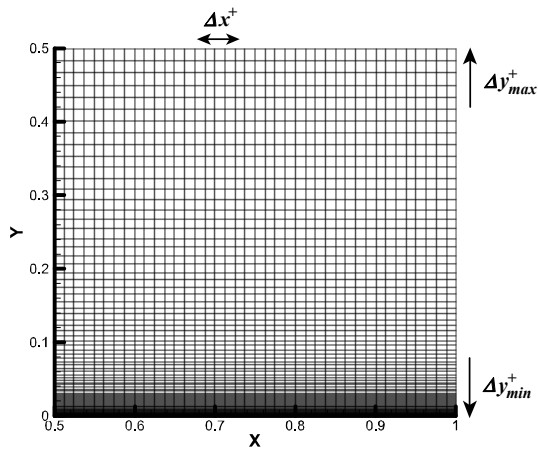


Fig. 1 Grid for manufactured solutions.

Table 3. Number of grid points with the grid spacing in each direction for manufactured solutions.

	$N_x \times N_y$	Δx^+	Δy_{min}^+	Δy_{max}^+
GMS1	161×321	9.39	0.25	12.55
GMS2	141×281	10.73	0.29	14.34
GMS3	121×241	12.52	0.34	16.73
GMS4	101×201	15.02	0.40	20.08
GMS5	81×161	18.78	0.51	25.10
GMS6	61×121	25.04	0.68	33.46

IV RESULTS AND DISCUSSION

A. Manufactured solution

1) Grid Description

Structured, orthogonal grids are prepared for manufactured solutions as shown in Fig. 1. Uniform grids are generated in the x -direction, while nonuniform grids with a hyperbolic tangent distribution are employed in the y -direction for denser meshes near the bottom wall. The number of grid points and the grid spacing in wall units are given as Table 3. For the geometrical similarity, the stretching parameter of the hyperbolic tangent function is kept constant for all grids.

2) Uncertainty Analysis

Figure 2 shows the convergence behavior of the friction resistance at the bottom under each condition. It is seen that, in Cases V(MS1) and VT(MS1), the results for the coarsest grid (GMS6) are apparently out of the asymptotic region. Therefore, the uncertainty is estimated using GMS1-5 throughout the present calculation, although the number of the data points for the Richardson extrapolation may not be enough for rigorous precision. The error of the calculated values with the finest grid from the exact solution is 1.18%, 21.1% and 21.9% for Cases V(MS2), V(MS1) and VT(MS1), respectively. The convergence behavior of each profile is as reasonable as expected from the formal order of accuracy of the present solver.

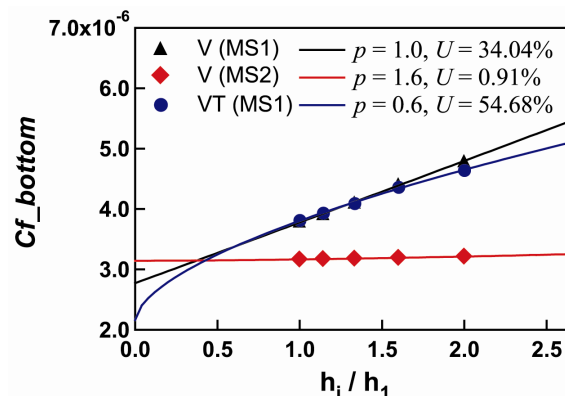


Fig. 2 Convergence of the friction resistance at the bottom wall.

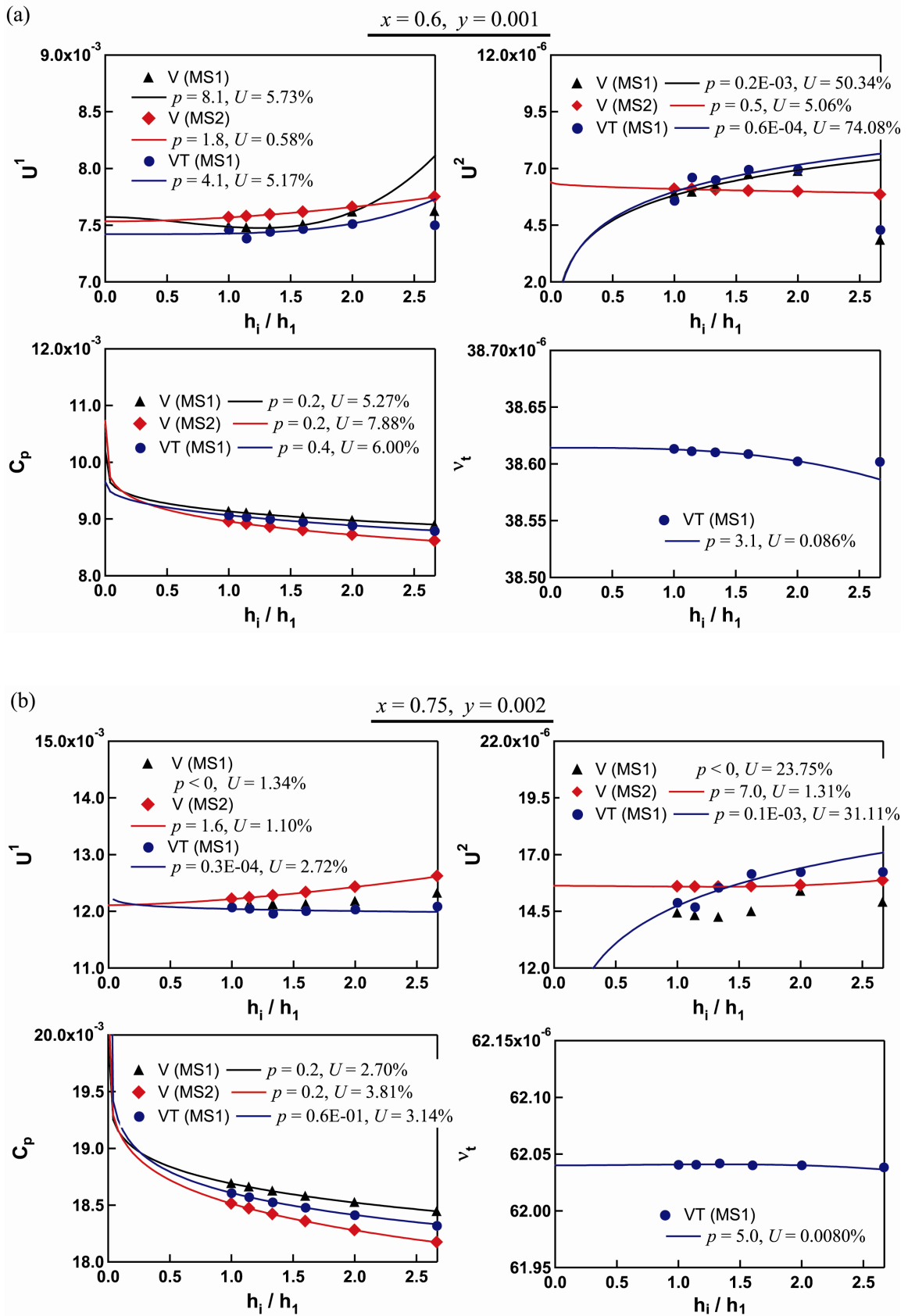


Fig. 3 Convergence of the local flow quantities at the three prescribed locations: (a) $x = 0.6, y = 0.001$, (b) $x = 0.75, y = 0.002$, (c) $x = 0.9, y = 0.2$.

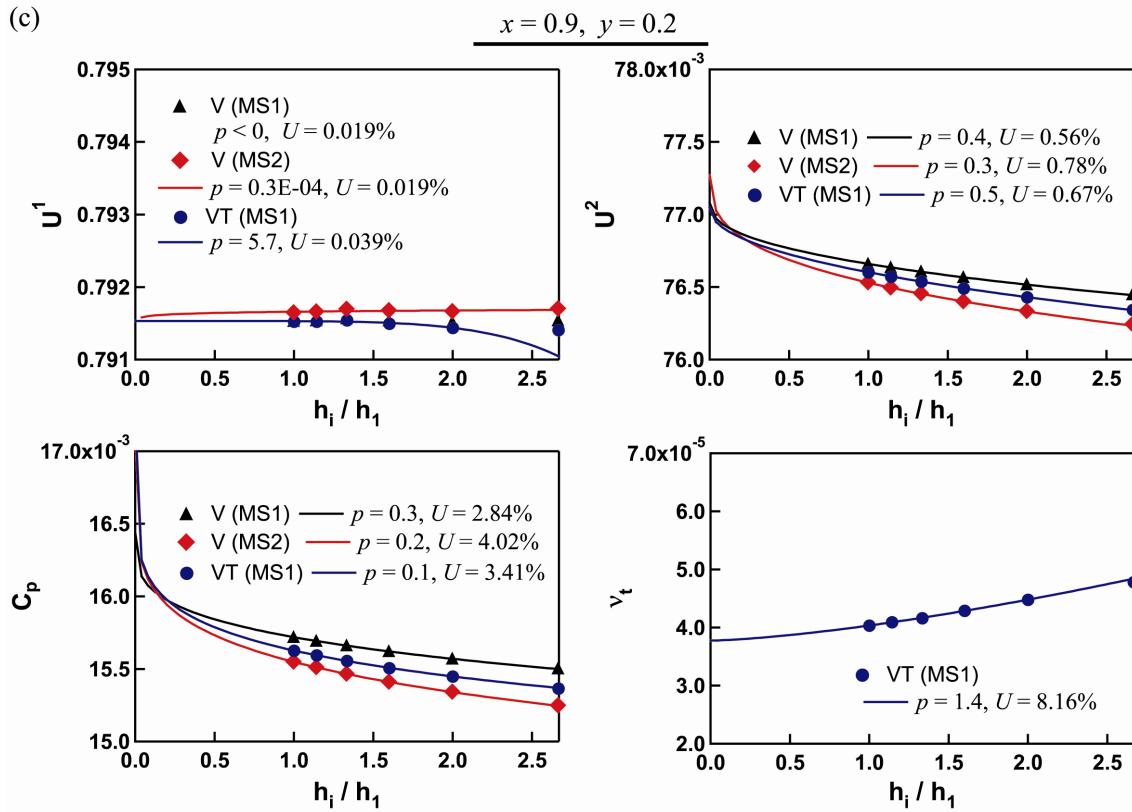


Fig. 3 (Cont.)

Table 4. Numerical error of calculated values from exact solutions.

Error (%)	$x = 0.6, y = 0.001$			$x = 0.75, y = 0.002$			$x = 0.9, y = 0.2$		
	V(MS2)	V(MS1)	VT(MS1)	V(MS2)	V(MS1)	VT(MS1)	V(MS2)	V(MS1)	VT(MS1)
U^1	0.61	0.45	0.82	1.50	0.79	0.28	0.0469	0.0324	0.032
U^2	2.85	6.19	11.03	2.84	10.1	7.24	0.663	0.496	0.57
C_p	6.85	4.99	5.70	3.44	2.52	3.14	3.72	2.66	3.24
v_t	—	—	2.18×10^{-3}	—	—	2.97×10^{-4}	—	—	9.39

Figure 3 shows the convergence behavior of the local flow quantities at the three prescribed locations. In Case V(MS2), all profiles are considered to be in the asymptotic range and exhibit favorable convergence behavior. On the other hand, in Cases V(MS1) and VT(MS1), the profiles of the velocity components exhibit unexpected behavior especially in the vicinity of the wall as shown in Figs. 3a and 3b.

It is noted that, in Fig. 3, large p (> 2) or small p (~ 0) corresponds to almost grid-independent behavior of the calculated values in Case V(MS2). Moreover, the accuracy of the post-processing of the data is first order in the present analysis. Thus, the results for Case V(MS2) would be quite reasonable for the friction resistance. The observed order of accuracy of the local flow quantities, however, is lower than expected. The reason of this deterioration of the grid convergence requires further investigation.

In Cases V(MS1) and VT(MS1), large or small values of p are mainly due to the awkward behavior of the profiles. It is conjectured that this unfavorable behavior of Case V(MS1) might come from the inconsistency of the second-order discretization of the present solver and the first-order source function added to the momentum equation in a volumetric form.

In Case VT(MS1), the reason of the non-monotonic behavior would be more complex. As mentioned by Eça et al. [1], the near-wall destruction term, of which the value is constant near the wall with MS1, is considered to be responsible for the numerical instability also in the present simulation. However, the cause is not yet specified, and further investigation is also necessary for results with the MS1 profile.

The numerical errors of calculated values from exact manufactured solutions are shown for the finest grid (GMS1) in Table 4. The discrepancy for the pressure and wall-normal velocity is quite large near the wall. The absolute error decreases with the grid refinement, but the convergence of the error field is not satisfactory both in the local and global sense for some unknown factors in the present results.

B. Backward facing step

1) Grid Description

For the simulation of the flow over a backward facing step, a set of orthogonal grids are prepared as shown in Fig. 4. The whole computational domain consists of three blocks. Nonuniform grids with a hyperbolic tangent distribution are employed both in the x - and y - directions for denser meshes near the wall and the upper corner of the step. The number of grid points and the grid spacing in wall units are given in Table 5.

2) Uncertainty Analysis

All the grids in Table 5 are used for the uncertainty estimation. Figure 5 shows the computed results of the integral quantities with the grid refinement. The observed order of accuracy and the estimated uncertainty for the finest grid are also labeled in the figure. Good convergence with the uncertainty being less than 1% of the extrapolated value is attained in all the quantities except for the reattachment point, which exhibits some oscillatory behavior.

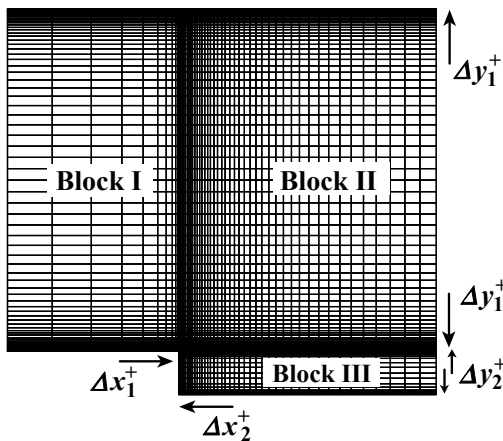


Table 5. Number of grid points with the grid spacing in each direction for the backward facing step.

	$(N_x \times N_y)_{I,II,III}$	Δx_1^+	Δx_2^+	Δy_1^+	Δy_2^+
GBS1	51×401, 401×401, 401×101	8.69	10.37	2.09	1.09
GBS2	41×321, 321×321, 321×81	11.01	12.98	2.62	1.38
GBS3	31×241, 241×241, 241×61	15.01	17.36	3.51	1.88
GBS4	21×161, 161×161, 161×41	23.55	26.18	5.32	2.94

Fig. 4 Magnified view of the grid system for the backward facing step.

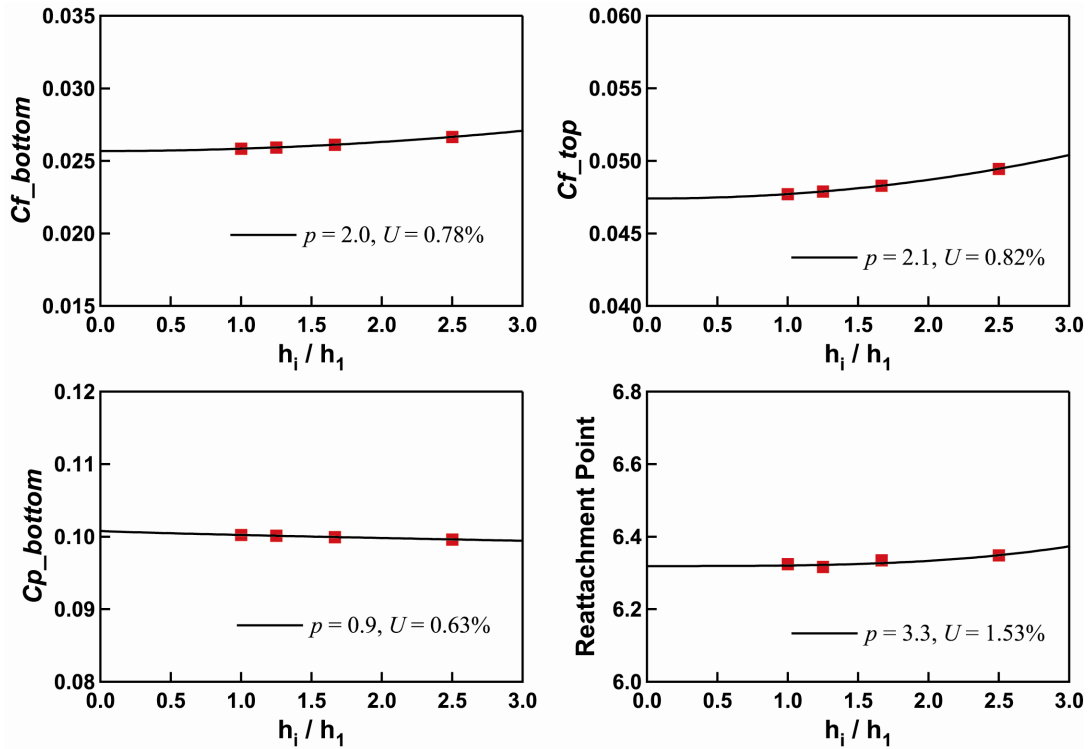


Fig. 5 Convergence of the integral quantities: friction resistance of the bottom wall (C_{f_bottom}) and the top wall (C_{f_top}), pressure resistance of the bottom wall (C_{p_bottom}), and reattachment point.

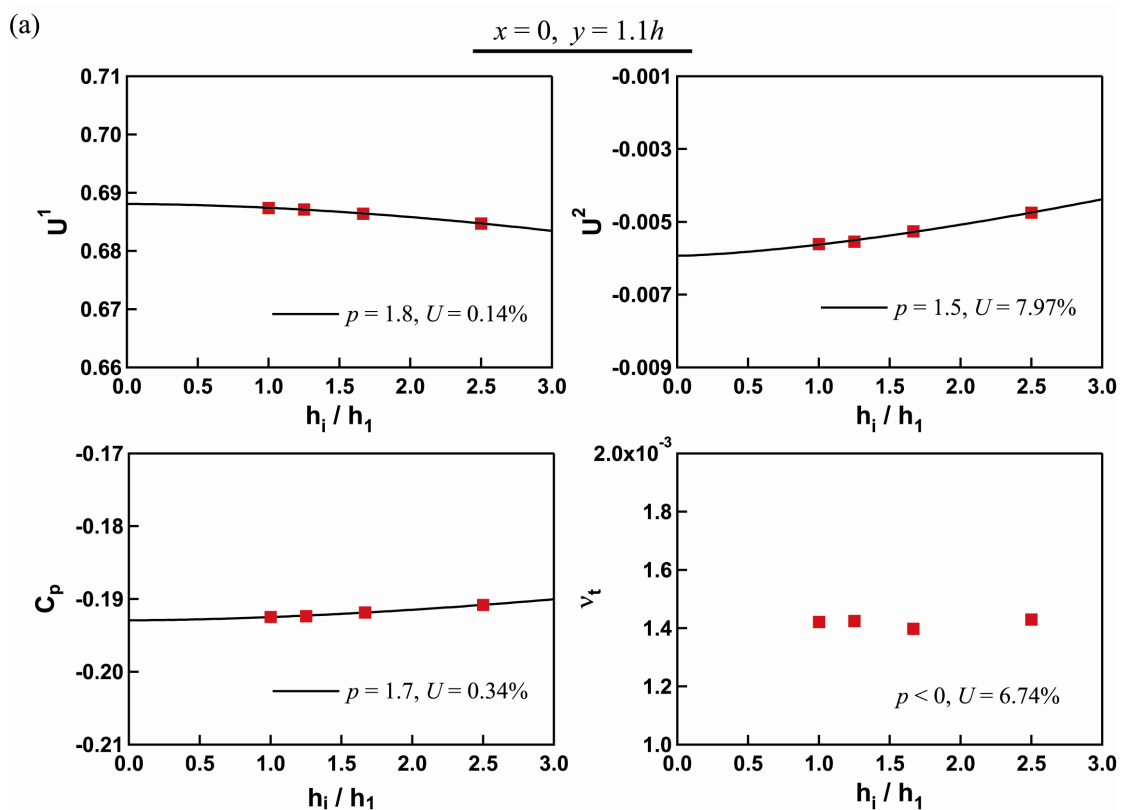


Fig. 6 Convergence of the local flow quantities at the three prescribed locations: (a) $x = 0, y = 1.1h$, (b) $x = h, y = 0.1h$, (c) $x = 4h, y = 0.1h$.

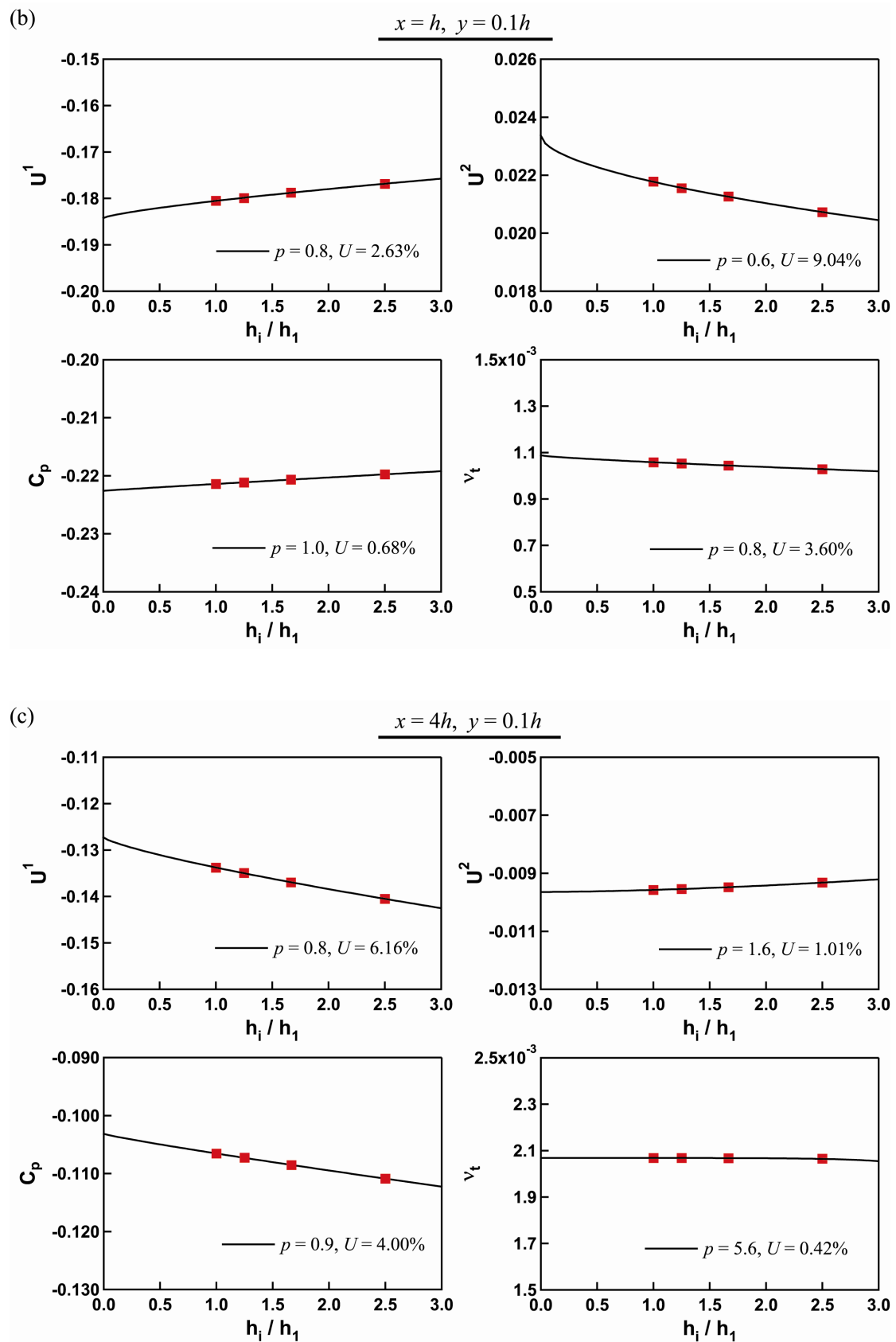


Fig. 6 (Cont.)

Figure 6 shows the convergence behavior of the local flow quantities at the three prescribed locations. For the velocity and pressure fields, favorable convergence is obtained with the observed order of accuracy between 0.5 and 2. The eddy-viscosity field, on the other hand, exhibits some peculiar tendency: oscillation near the separation point (Fig. 6a), expected behavior with the first-order discretization (Fig. 6b), and almost constant values near the reattachment point (Fig. 6c).

The divergent case often appeared in the uncertainty estimation with the single-block grids employed in the last workshop [10], while the present analysis with orthogonal grids shows that most of the computed values are well in the asymptotic region.

V CONCLUSIONS

Two test case problems for the two-dimensional, steady, incompressible, turbulent flows were calculated by the Navier-Stokes solver SURF with Spalart-Allmaras one-equation turbulence model, and the numerical uncertainty estimation based on the GCI method was performed in order to investigate the grid convergence behavior.

The manufactured solutions in a square domain proposed by Eça et al. [1] are simulated under different conditions. For the computation of the velocity and pressure fields with the fixed eddy-viscosity field, the reasonable grid-convergence behavior is obtained for the integral quantity when the MS2 profile is employed. The convergence behavior is not satisfactory when the MS1 profile is used. For the full computation of the flow and eddy-viscosity fields by using MS1 only as the boundary condition, the similar tendency to the previous case (fixed eddy viscosity with MS1) is observed and the local flow quantities are not completely converged. In each case, the computed values converge toward the manufactured solution, while the grid-convergence behavior that is expected from the formal order of accuracy has not yet been obtained by the present solver, and the observed accuracy of the local flow quantities is somewhat lower than expected.

The turbulent flow over a backward facing step (ERCOFTAC Database, Case-30) is also performed by using the SURF solver. Most of the present results obtained with orthogonal grids are considered to be in the asymptotic region.

REFERENCES

- [1] L. Eça, M. Hoekstra, A. Hay, and D. Pelletier, "Manufactured Solutions for One-Equation Turbulence Models in a Two-Dimensional Steady Wall-Bounded Incompressible Turbulent Flow," IST Report D72-36, EPM-RT-2006-02, 2006.
- [2] L. Eça and M. Hoekstra, "Uncertainty Estimation: A Ground Challenge for Numerical Ship Hydrodynamics," 6th Numerical Towing Tank Symposium, Rome, 2003.
- [3] L. Eça, and M. Hoekstra, "An Evaluation of Verification Procedures for CFD Applications," 24th Symp. on Naval Hydro., Fukuoka, 2002.
- [4] P. J. Roache, *Verification and Validation in Computational Science and Engineering*, Hermosa Publishers, 1998.
- [5] T. Hino, "A 3D Unstructured Grid Method for Incompressible Viscous Flows," J. Soc. Naval Archit. Japan, Vol. 182, pp. 9-15, 1997.
- [6] A. J. Chorin, "A Numerical Method for Solving Incompressible Viscous Flow Problems," J. Comput. Phys., Vol. 2, pp. 12-26, 1967.

- [7] P. R. Spalart and S. R. Allmaras, "A One-Equation Turbulence Model for Aerodynamic Flows", AIAA 30th Aerospace Sciences Meeting, AIAA Paper 92-0439, Reno, NV, 1992.
- [8] P. L. Roe, "Characteristic-Based Scheme for the Euler Equations," *Ann. Rev. Fluid Mech.*, Vol. 18, pp. 337-365, 1986.
- [9] B. Van Leer, "Toward the Ultimate Conservative Difference Scheme V: A Second-Order Sequel to Godunov's Method," *J. Comput. Phys.*, Vol. 32, pp. 101-136, 1979.
- [10] Y. Sato and T. Hino, "Navier-Stokes Computations of Ship Flows on Unstructured Grids," Workshop on CFD Uncertainty Analysis, Lisbon, 2004.